ELSEVIER

Journal of Power Sources 74 (1998) 202–210

JOURNAL OF POWER SOURCES

Thermal behaviour of nickel/metal hydride batteries during charge and discharge

M.S. Wu, Y.Y. Wang *, C.C. Wan

Department of Chemical Engineering, National Tsing-Hua University, Hsinchu 30043, Taiwan

Received 14 January 1998; accepted 10 February 1998

Abstract

This work employs a one-dimensional and a two-dimensional model to predict the thermal behaviour of 30-A h Ni/MH batteries. The temperature of battery can rise to about 45°C during 15-A charging under natural convection. Batteries attached with aluminum fins exhibit an effective heat-dissipation behaviour under either natural convection or forced convection conditions. The temperature is around 37 and 32°C under natural convection and forced convection, respectively. During discharge, the temperature rise of the battery is only about 6°C under adiabatic conditions. In a closely-packed module, natural and forced convection is unable to reduce the temperature increase in the central part of a module. Experimental results indicate that the one-dimensional model is sufficient for the system operating under natural convection condition. For forced convection, the prediction is more accurate with the two-dimensional model. In general, the simulation results correlate well with measurements.

Keywords: Nickel/metal hydride battery; Mathematical model; Metallic fin

1. Introduction

Rechargeable Ni/MH batteries are becoming increasingly popular owing to the demand for power sources with high specific energy, high-rate capability, long cycle life, and low environmental impact. Ni/MH batteries are also highly promising for electric vehicles [1].

To achieve the required capacity, a large-scale battery is necessary for electric-vehicle applications. The temperature tends to increase in electric-vehicle batteries during charging and discharging processes. With lead/acid batteries, high temperatures might cause the electrolyte to become more corrosive and the charging current to become unstable. Moreover, the structure of the active materials in the positive electrode might degrade and, ultimately, becomes inactive [2]. Such effects decrease the battery capacity and shorten the cycle life [3]. Similarly, many serious problems attributed to high temperature also arise in lithium batteries. For instance, a situation in which the generated heat during discharging cannot be effectively removed might create either an irreversible side reaction in the batteries or melting of the solid lithium [4]. The above two examples demonstrate that high temperature can heavily influence the performance of batteries, particularly in large units.

The mathematical simulation of heat transport in batteries is an effective means of obtaining information on whether or not excessive heat can be removed, or how operating temperature can be controlled in an appropriate range. Several studies have closely examined the thermal behaviour of electric-vehicle batteries. Pal and Newman [4,5], Newman and Tiedeman [6] and Chen and Evans [7–9] have presented mathematical models to calculate the thermal behaviour of a lithium/polymer battery. Choi and Yao [3,10] have developed a mathematical model for the lead/acid battery. Lee et al. [11] have also proposed a mathematical model for electric-vehicle batteries.

While focusing primarily on lead/acid and lithium/polymer batteries, most of the above studies have not addressed the thermal behaviour of the Ni/MH system, which is particularly sensitive to elevated temperature. Therefore, in this study, we employ one-dimensional and two-dimensional mathematical models to predict the thermal behaviour of Ni/MH batteries. The results are compared with actual measurements. Consideration is also given to the fact that, in practical electric-vehicle applications, batteries are connected either in series or parallel to provide the required voltage and capacity, Consequently,

* Corresponding author.

the heat dissipation from 20 single Ni/MH batteries connected in a series is examined. Finally, the feasibility of using metallic fins to accelerate heat dissipation is explored.

2. Experimental

A 30-A h, Ni/MH cell (110 × 20 × 90 mm) fabricated by NEXcell Battery, was used as a test unit to investigate the temperature distribution during discharging and charging. The electrodes were encased in a container made of stainless steel.

Charging and discharging were controlled at constant current by a charge/discharge unit (Kikusui PFX40 W-8). The cut-off of the discharge voltage was 1.0 V. The temperature variations in different locations during charging and discharging were measured by 12 thermocouples (K-type, diameter 0.12 mm) embedded inside the battery. The data were recorded on a personal computer with an amplifier board (Adventech PCLD-779) and a data-acquisition card (Adventech PCL-812PG).

Owing to the lack of information of some thermophysical parameters, the Knodler [12] method and the thermal conductivity measuring apparatus were employed to estimate the heat capacity and the thermal conductivity, respectively. Measurements of thermal conductivity, obtained by means of a Tokyo Meter HVS-40-200 SD were taken before cycling. The electrodes are porous materials and are filled with air during measurement. Finally, the porosity of the electrode materials and the separator was measured by means of mercury porosimetry (Micromeritics Autopore II 9220).

3. Results and discussion

A Ni/MH cell can be conceptually divided into two regions: a core region and a boundary region (as in the two-region model of Lee et al. [11]). The core region is composed of electrode materials, a separator, and an electrolyte. The boundary region is the stainless-steel case. The 30-A h Ni/MH cell is shown schematically in Fig. 1. In our system, the heat dissipation in the *y*-direction is larger, and therefore, more critical than in other directions. Nevertheless, the heat dissipation in the *x*-direction is also examined in order to yield more accurate results. The density, thermal conductivity and heat capacity of the

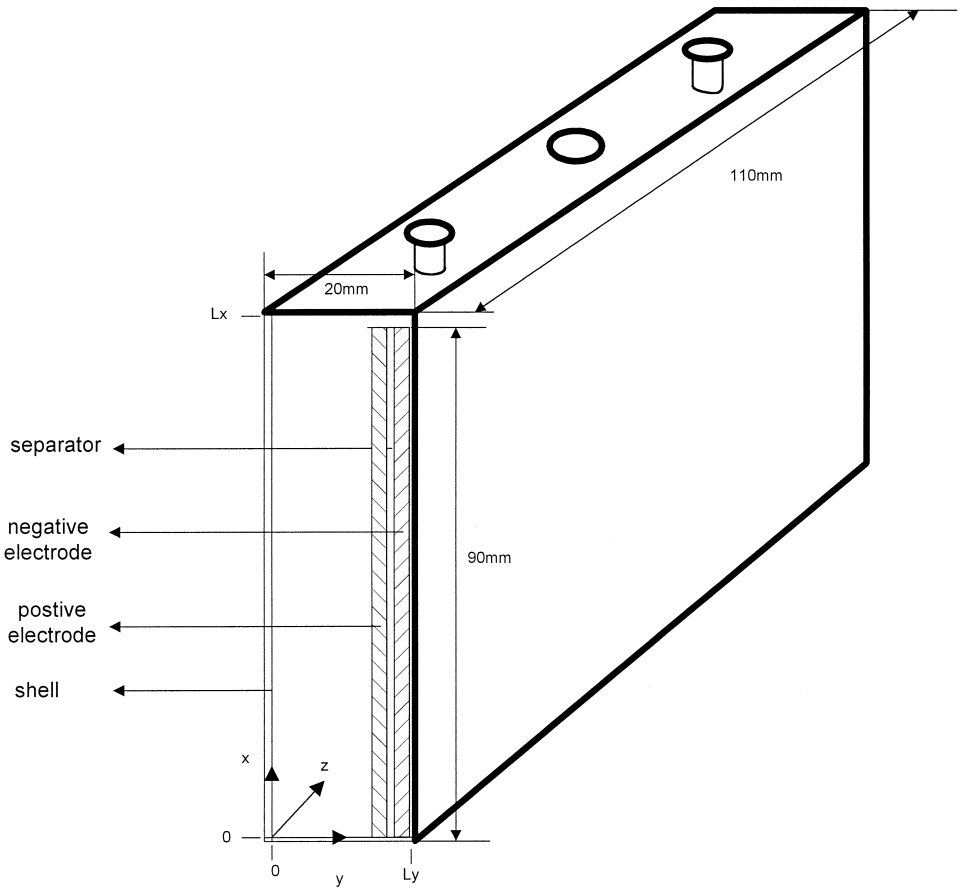

Fig. 1. Schematic of a 30-A h Ni/MH cell.

electrode are assumed to remain constant within a certain temperature range. The motion of the electrolyte due to the change in electrode, porosity is neglected. Based on these assumptions, the transient heat transfer model, i.e., either a one-dimensional or a two-dimensional heat transfer model, can be written as:

$$\text{one-dimensional model: } \rho C_p \frac{\partial T}{\partial t} = k_y \frac{\partial^2 T}{\partial y^2} + \dot{q} \qquad (1)$$

$$\text{two-dimensional model: } \rho C_p \frac{\partial T}{\partial t} = k_x \frac{\partial^2 T}{\partial x^2} + k_y \frac{\partial^2 T}{\partial y^2} + \dot{q} \qquad (2)$$

where ρ denotes the average density (3250 kg/m^3); C_p represents the average heat capacity; k_x and k_y is the thermal conductivity of the battery in the x-direction and the y-direction, respectively; $\dot{q}$ denotes the rate of heat generation per unit volume. For simplicity, according to the assumption of Bernardi et al. [13], the heat generation is distributed uniformly throughout the battery. Hence, heat generation can be written as:

$$\dot{q} = \frac{I}{V_b}\left[(E - E_0) + T\frac{dE_0}{dT}\right] \qquad (3)$$

where: I represents the current ($I > 0$ for charging and $I < 0$ for discharging), V_b is the cell volume, E denotes the cell potential; E_0 represents the open-circuit potential.

According to Berndt [14], the heat generation can be divided into the joule effect $(E - E_0)$ and the reversible heat effect $(T\,dE_0/dT)$. In a Ni/MH battery, the reversible heat effect is attributed primarily to the hydrogen absorbing–desorbing reaction on the negative electrode during cycling [14]; the joule heat effect is ascribed largely to the charging reaction. As the battery approaches 75 ~ 80% state-of-charge, oxygen evolution occurs at the positive electrode and oxygen reduction at the negative electrode [15]. In this 'internal oxygen cycle reaction' [14], the reversible heat effects at the positive and negative electrode cancel out each other, and the open-circuit voltage equals zero [14]. Consequently, in our models, the total charging current (I) is divided into two parts: the current of charging reaction (I_1) and the current of the internal

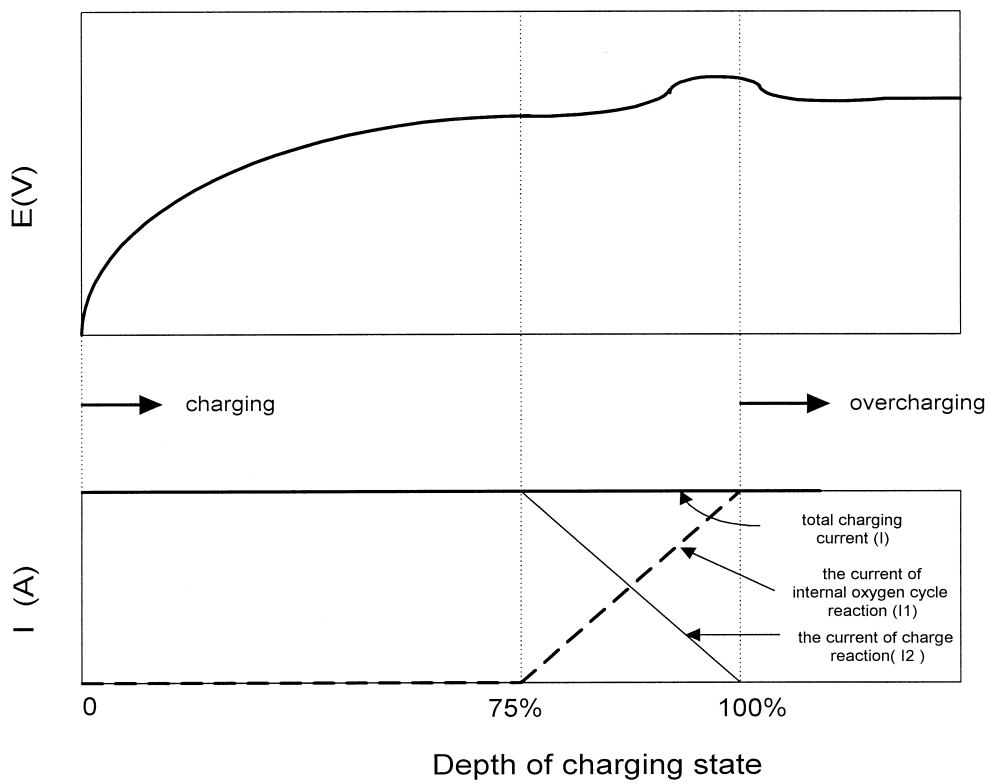

Fig. 2. Current and voltage curves of a Ni/MH cell during charging.

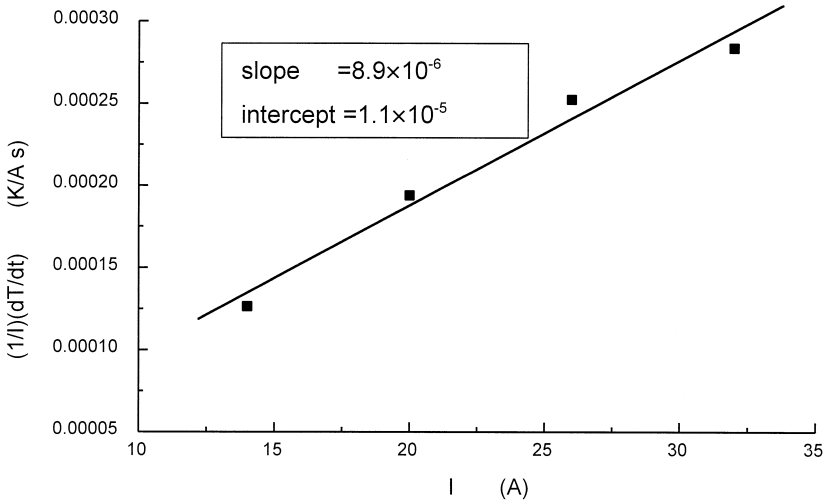

Fig. 3. Relationship of $(1/I)(\mathrm{d}T/\mathrm{d}t)$ and charging current I.

oxygen cycle reaction (I_2). A typical current response during charging, is shown in Fig. 2.

It is further assumed that only convection cooling is significant at the boundary and radiation cooling can be neglected. Assuming a constant heat transfer coefficient over the battery external surface, the boundary conditions can be written as follows [11]:

$$-k_x\frac{\partial T}{\partial x}=\left[\frac{L_\mathrm{A}}{k_\mathrm{A}}+\frac{1}{h}\right]^{-1}(T-T_\infty)$$
$$\text{at } x=0,\ 0<y<L_y \tag{4}$$

$$-k_x\frac{\partial T}{\partial x}=\left[\frac{L_\mathrm{A}}{k_\mathrm{A}}+\frac{1}{h}\right]^{-1}(T-T_\infty)$$
$$\text{at } x=L_x,\ 0<y<L_y \tag{5}$$

$$-k_x\frac{\partial T}{\partial x}=\left[\frac{L_\mathrm{A}}{k_\mathrm{A}}+\frac{1}{h}\right]^{-1}(T-T_\infty)$$
$$\text{at } y=0,\ 0<x<L_x \tag{6}$$

$$-k_y\frac{\partial T}{\partial x}=\left[\frac{L_\mathrm{A}}{k_\mathrm{A}}+\frac{1}{h}\right]^{-1}(T-T_\infty)$$
$$\text{at } y=L_y,\ 0<x<L_x \tag{7}$$

where: L_A (0.5 mm) denotes the thickness of the wall; k_A (468 J/kg K) represents the thermal conductivity of the wall; T_∞ is the ambient temperature. Boundary conditions (6) and (7) are for a one-dimensional model, and boundary conditions (4) ~ (7) are necessary for a two-dimensional one.

In this study, the battery was kept at ambient temperature prior to charging and discharging. Therefore, the initial condition can be written as

$$T=T_\infty \qquad t=0,\ 0<x<L_x,\ 0<y<L_y. \tag{8}$$

Owing to the lack of published data, Eq. (9) [12] can be used to determine the actual heat capacity and reversible heat effects of battery, viz.,

$$\frac{1}{I}\frac{\mathrm{d}T}{\mathrm{d}t}=\frac{R_\mathrm{z}}{mC_\mathrm{p}}I-\frac{T}{mC_\mathrm{p}}\frac{\mathrm{d}E_0}{\mathrm{d}T} \tag{9}$$
$$R_\mathrm{z}=\frac{\eta}{I}$$

where: R_z denotes the apparent DC cell resistance; m represents the total mass of the battery; η is the overvoltage.

The relationship between $(1/I)(\mathrm{d}T/\mathrm{d}t)$ and the charging current I is shown in Fig. 3. According to the slope and the intercept, the heat capacity and reversible heat effects $(T\mathrm{d}E_0/\mathrm{d}T)$ of the battery are equal to 2788 J/kg K and 0.023 V, respectively. The measured heat capacity includes the core and the wall regions but the average heat capacity of the core region can be estimated as 3200 J/kg K.

Based on the concept of equivalent electric resistance connected in a series- or parallel-form, in this work, k_x and k_y are estimated according to the following equations [8]:

$$\text{series-connected } k_y=\frac{L_y}{\sum_i\frac{Ly_i}{k_i}}=\frac{L_y}{\frac{Ly_\mathrm{p}}{k_\mathrm{p}}+\frac{Ly_\mathrm{n}}{K_\mathrm{n}}+\frac{Ly_\mathrm{s}}{k_\mathrm{s}}} \tag{10}$$

$$\text{parallel-connected } k_x=\sum_i\frac{k_iLy_i}{Ly}=\frac{k_\mathrm{p}Ly_\mathrm{p}+k_nLy_\mathrm{n}+k_\mathrm{s}Ly_\mathrm{s}}{Ly} \tag{11}$$

where: Ly_p, Ly_n and Ly_s denote the total thickness (mm) of positive electrode, negative electrode, and separator, respectively; k_p, k_n and k_s represent the average thermal

Table 1
Average thermal conductivities of electrodes and separator

	Positive electrode	Negative electrode	Separator
k_m (W/m K)	1.14[a]	1.16[a]	0.22[b]
ε (porosity)	0.22[c]	0.27[c]	0.74[c]
$k_m[1-\varepsilon]$ (W/m K)	0.89[a]	0.85[a]	0.057
k_f (W/m K)	0.57[d]	0.57[d]	0.57[d]
Ly_i (mm)	7.37	5.40	6.23
k (W/m K)	1.02*	1.00*	0.48*

[a] Measured result.
[b] Ref. [14].
[c] Measured result.
[d] Ref. [16].
* The average thermal conductivity is estimated by Eq. (12) [16]:

$$k = k_m(1-\varepsilon) + k_f\varepsilon \quad (12)$$

where k_m, and k_f are the thermal conductivities of structural materials and filling material (KOH), respectively.

conductivities (W/m K) of positive electrode, negative electrode and separator, respectively. Table 1 summarizes the average thermal conductivities of the electrodes and the separator. The k_y and k_x are estimated to be 0.72 and 0.84 W/m K, respectively.

The voltage response of the 30-A h Ni/MH cell during 15 and 20 A charging is given in Fig. 4. This voltage response is then used in Eq. (3) to calculate the value of the joule effect. Part of the joule effect due to the charging reaction equals $(E-E_0)\times I_1$ and the other part due to the internal oxygen cycle reaction equals $(E-E_0)\times I_2$. Consequently, the joule effect can be described as $0.3\times I_1 + 1.5\times I_2$ at 15 A charging. Notably, the reversible heat effect $(T[\mathrm{d}E_0/\mathrm{d}T]\times I_1)$ is only $0.023\times I_1$. Moreover, the rate of heat generation during charging is attributed primarily to the joule effect, particularly above 75% state-of-charge.

The finite difference method is employed to derive the two mathematical models. Fig. 5 presents the calculated (one-dimensional and two-dimensional models) and measured temperature profile in the *x*- and *y*-directions at varying charging times under natural convection. When the charging times are 60 and 90 min, the battery temperature rises from 23.5 to 28.5 and 32.5°C, respectively. Simulation results correlate fairly well with the actual temperature distribution. Towards the end of the charging stage (114 min), however, the measured temperature distribution apparently becomes less uniform than predicted. Fig. 5 also reveals that the calculated temperature profile, as obtained by the one-dimensional model, is close to the two-dimensional model in the *y*-direction under natural convection. This finding suggests that the one-dimensional model can predict accurately the temperature distribution under natural convection in our system.

Fig. 6 compares the one-dimensional and two-dimensional mathematical models in terms of the calculated temperature rise in the centre of the battery under natural or forced convection. According to this comparison, the one-dimensional and two-dimensional models tend to differ less in terms of temperature rise as the heat transfer coefficient at the external surface is decreased from 25 to 6 W/m^2 K. In addition, comparing forced and natural convections indicates that the battery temperature is markedly lower under forced convection than under natural convec-

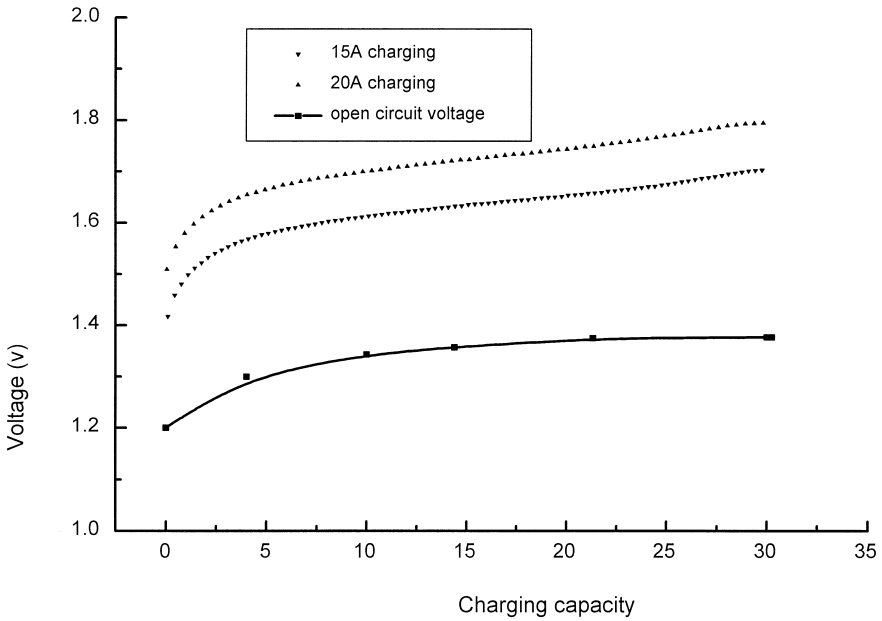

Fig. 4. Voltage response of a 30-A h Ni/MH cell during charging at 15 and 20 A.

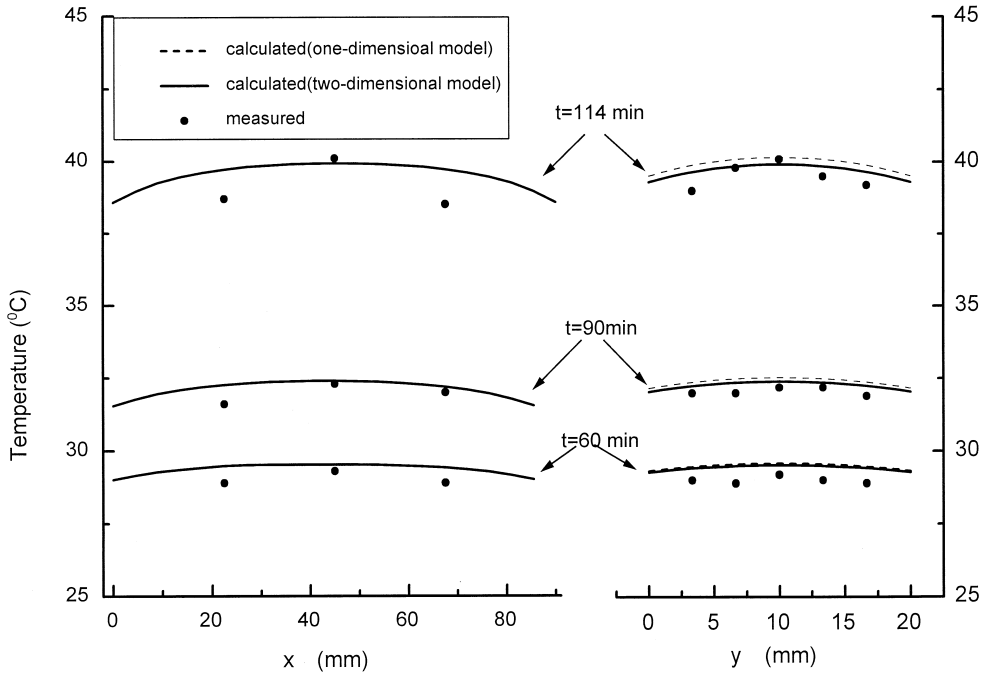

Fig. 5. Measured and calculated (one-dimensional and two-dimensional models) temperature profile in x-and y-directions at varying charging times under natural convection ($h = 6$ W/m^2 K); charging current 15 A.

tion. This discrepancy is ascribed to the fact that forced convection can sufficiently dissipate the generated heat. The one-dimensional model becomes less accurate than the two-dimensional model under forced convection.

The two-dimensional temperature distribution at the end of charging at 15 A under natural or forced convection is shown in Fig. 7. When the charging process is under natural convection, the temperature gradient in the x-direction is not as pronounced as that under forced convection. Therefore, the heat dissipation effect in the x-direction can be neglected in comparison with the y-direction. This phenomenon indicates that the one-dimensional model can

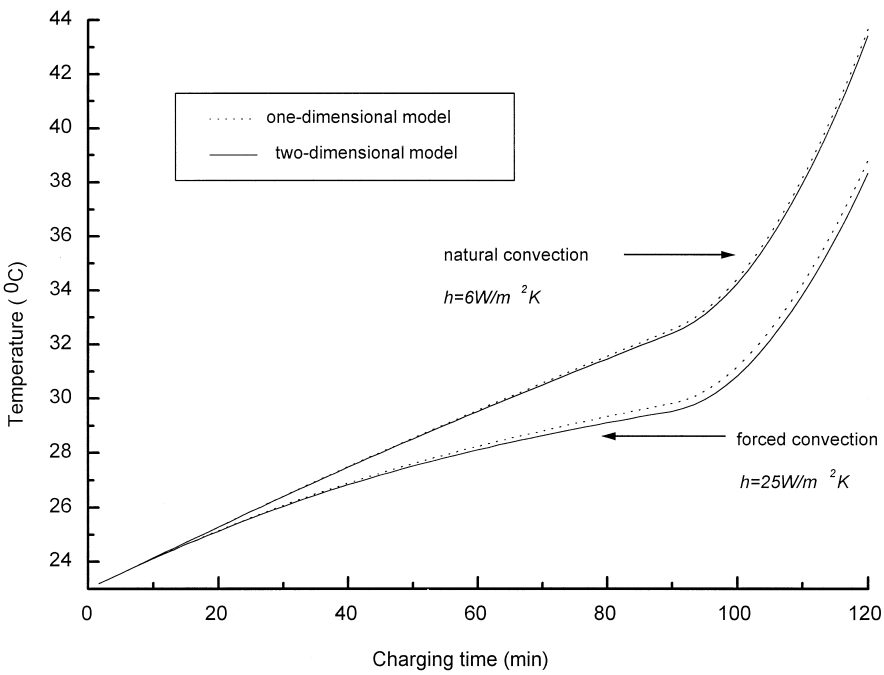

Fig. 6. Calculated temperature rise in the centre of a cell by means of one-dimensional and two-dimensional mathematical models for charging at 15 A.

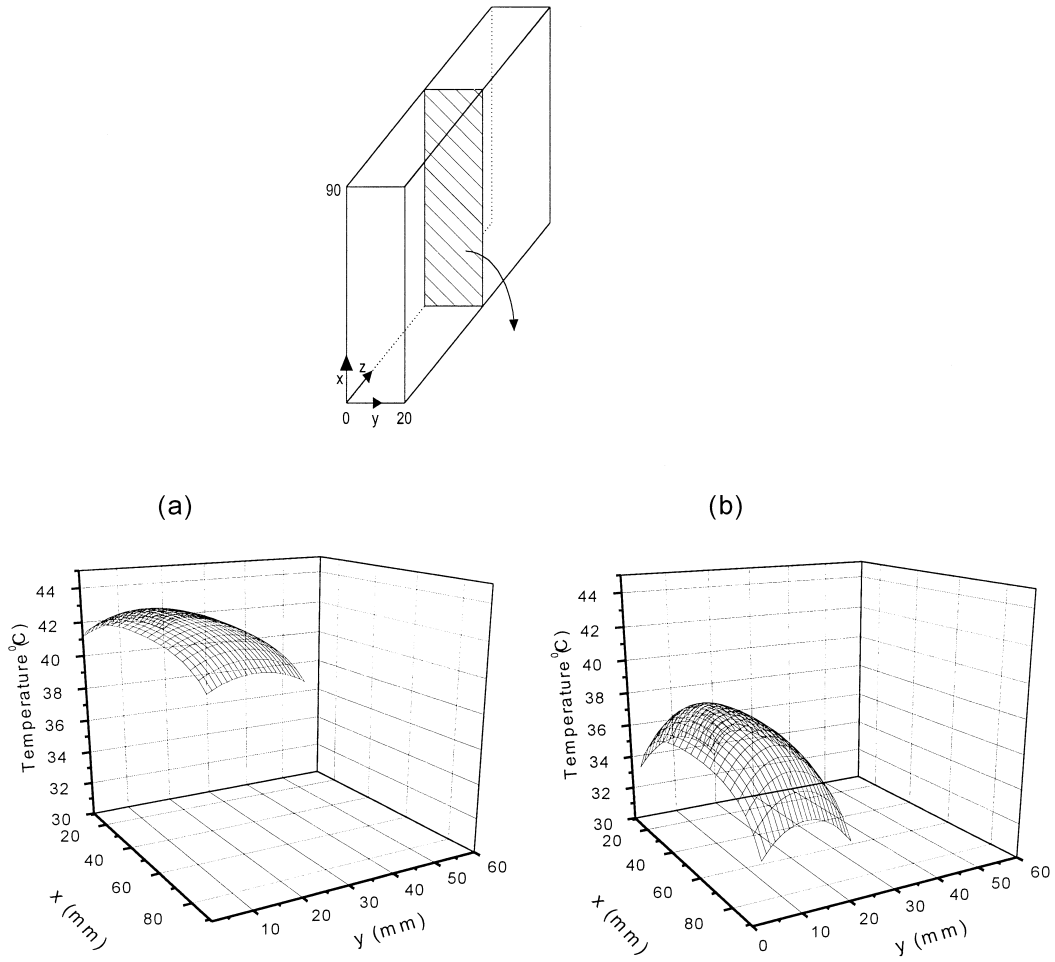

Fig. 7. Temperature distribution at the end of charging at 15 A by means of two-dimensional model under: (a) natural convection ($h = 6$ W/m^2 K); (b) forced convection ($h = 25$ W/m^2 K).

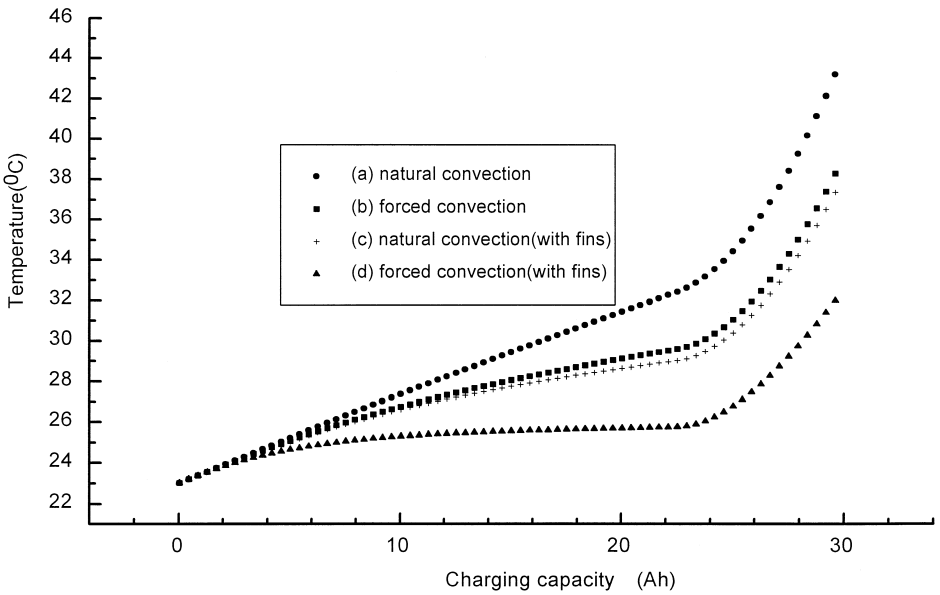

Fig. 8. Calculated temperature rise in the centre of a 30-A h Ni/MH cell during charging at 15 A for four different cooling situations.

describe adequately the battery temperature distribution under conditions of a low heat transfer coefficient. The heat dissipation increases in the *x*-direction, however, on increasing the heat transfer coefficient. The heat dissipation cannot be neglected because the temperature gradient becomes larger. Thus, the two-dimensional model is deemed necessary to investigate the thermal behaviour under forced convection.

Previous studies [16,17] have demonstrated that a metallic fin can effectively enhance the rate of heat dissipation. Therefore, in this work, we examined the effect of adding an aluminum fin to the Ni/MH battery. The fins consisted of 100 sheets ($110 \times 2.5 \times 0.25$ mm for each sheet) and were used on the two external surfaces in the *y*-direction. Fig. 8 gives the temperature rise in the central region of a 30-A h Ni/MH cell during charging at 15 A under four different cooling cases: (a) natural convection; (b) forced convection; (c) natural convection (with fins); (d) forced convection (with fins). Comparison between (a) and (c) or (b) and (d) reveals that either in natural convection or forced convection, the aluminum fins can reduce significantly the temperature rise due to the increase in the heat dissipation surface. In case (d), the temperature rise decreases rapidly and the temperature quickly reaches a steady value before 75% state of charging. Beyond this state, the temperature increases due to the internal oxygen cycle reaction. Nevertheless, the temperature is still markedly lower than in cases (a), (b) and (c).

On discharge, the results demonstrate that the increased temperature is only $\sim 6^{\circ}C$ after full discharge under adiabatic conditions. If convection cools the external surface, then the temperature will be much lower. This indicates that the temperature rise during discharging is not a serious problem even under the worst heat-dissipation conditions.

Multiple batteries packed in a module naturally will have more serious heat-dissipation problems than a single battery system. Fig. 9 displays the simulated temperature distribution of a closely packed module (20 cells in series) at the end of charging at 15 A under (a) natural convection, (b) forced convection and (c) forced convection (with fins). Notably, the temperature in the centre of the module is roughly the same regardless of the convection mode. By contrast, the temperature in the centre of a single cell is substantially lower under forced convection than under

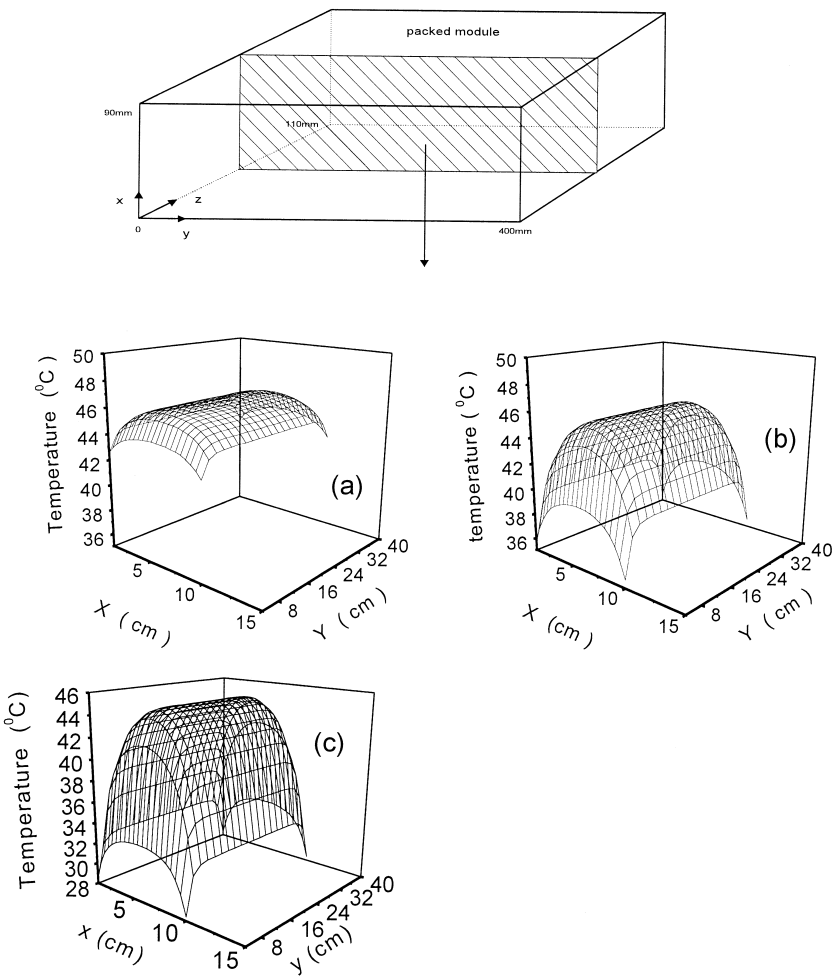

Fig. 9. Simulated temperature distribution of a closely packed module at the end of charging at 15 A and under (a) natural convection and (b) forced convection.

natural convection (Fig. 7). Obviously, both natural and forced convection cannot effectively reduce the temperature rise in the central region of a packed module. The scale of the packed module is much larger than the single cells in addition, the heat transfer resistance in the *y*-direction is larger. Therefore, the generated heat of the packed module in the central region is insufficiently dissipated to the surroundings by natural or forced convection. When metallic fins are used on the external surface of a packed module in the *y*-direction the data of Fig. 9c reveals that the temperature cannot be reduced, even with forced convection. To improve the heat dissipation of a closely packed module, aluminum fins are required together with adequate air space between each battery to facilitate further forced convection. Unfortunately, this approach is not practical.

4. Conclusions

Based on the results obtained from model prediction and experimental measurements, we can conclude the following.

(1) The one-dimensional model can accurately predict the temperature distribution of a 30-A h Ni/MH cell under natural convection. In addition, a two-dimensional model is required under forced convection. The predictions by both models correlate well with the measured temperature distribution under natural convection. However, as full charge is approached and the changing current increases to 20 A, the actual measured temperature distribution becomes less uniform than that of the prediction.

(2) The temperature rise of a battery in the charging process can reach around 45°C. Hence, the charging temperature becomes a major problem, particularly at 75% state of charge. Simulation results demonstrate that the heat dissipation can be effectively improved by attaching aluminium fins on the external surface of the battery. Moreover, the discharging temperature is not a serious problem because the increased temperature is only ~ 6°C at full discharge under adiabatic condition.

(3) In a closely packed module, natural and forced convection cannot effectively reduce the temperature rise in the centre of a battery module.

5. Symbols and nomenclature

C_p	Heat capacity (J/kg K)
E	Cell potential (V)
E_o	Open-circuit potential (V)
h	Heat transfer coefficient (W/m^2 K)
I	Current (A)
k_A	Thermal conductivity of wall (W/m K)
k_n	Thermal conductivity of negative electrode (W/m K)
k_p	Thermal conductivity of positive electrode (W/m K)
k_s	Thermal conductivity of separator (W/m K)
k_x	Thermal conductivity in the *x*-direction (W/m K)
k_y	Thermal conductivity in the *y*-direction (W/m K)
L_A	Thickness of the wall (mm)
L_n	Total thickness of negative electrode (mm)
L_p	Total thickness of positive electrode (mm)
L_s	Total thickness of separator (mm)
L_x	Total thickness of battery in *x*-direction (mm)
L_y	Total thickness of battery in *y*-direction (mm)
m	Total mass of battery (kg)
$\dot{q}$	Heat generation rate per unit volume (J/m^3 s)
R_z	Apparent DC cell resistance (Ω)
T	Temperature of battery (°C)
T_∞	Ambient temperature (°C)
t	Time (s)
V_b	Cell volume (m^3)
ρ	Density (kg/m^3)
η	Overvoltage (V)

References

[1] S.R. Ovshinsky, M.A. Fetcenko, J. Ross, Science 260 (1993) 176.
[2] S.M. Caulder, A.C. Simon, J. Electrochem. Soc. 121 (1974) 1546.
[3] K.W. Choi, N.P. Yao, J. Electrochem. Soc. 125 (1978) 1011.
[4] C.R. Pal, J. Newman, J. Electrochem. Soc. 142 (1995) 3274.
[5] C.R. Pal, J. Newman, J. Electrochem. Soc. 142 (1995) 3282.
[6] J. Newman, W. Tiedeman, J. Electrochem. Soc. 142 (1995) 1054.
[7] Y. Chen, J.W. Evans, J. Electrochem. Soc. 140 (1993) 1833.
[8] Y. Chen, J.W. Evans, Electrochim.q Acta 39 (1994) 517.
[9] Y. Chen, J.W. Evans, J. Electrochem. Soc. 143 (1996) 2708.
[10] K.W. Choi, N.P. Yao, J. Electrochem. Soc. 126 (1979) 1321.
[11] J. Lee, K.W. Choi, N.P. Yao, C.C. Christianson, J. Electrochem. Soc. 133 (1986) 1286.
[12] R. Knodler, J. Appl. Electrochem. 13 (1984) 39.
[13] D. Bernardi, E. Pawlikowski, J. Newman, J. Electrochem. Soc. 132 (1985) 5.
[14] D. Berndt, Maintenance-Free Batteries, Wiley, New York, 1993.
[15] D. Linden, Handbook of Batteries, McGraw-Hill, New York, 2nd edn., 1994.
[16] J. Kim, T.V. Nguen, R.E. White, J. Electrochem. Soc. 139 (1992) 2781.
[17] Y. Cho, G. Halpert, J. Power Sources 18 (1986) 109.